

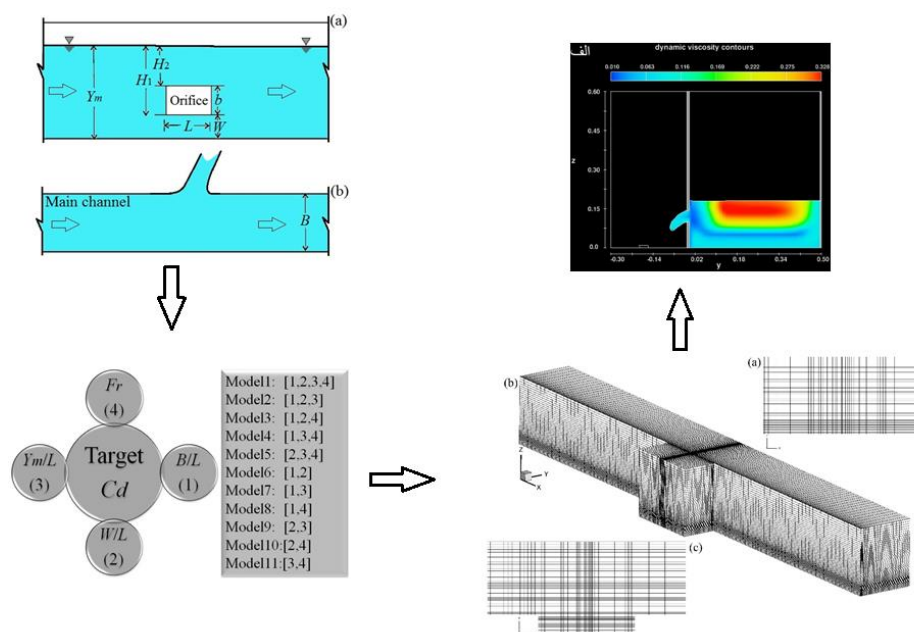
Effects of side orifice dimensions on characteristics of flow field in rectangular channels

Babak Sanahmadi¹, Majeid Heydari^{*,1}, Saeed Gohari¹, Saeid Shabanlou²

¹Department of Water Science and Engineering, Faculty of Agriculture, Bu-Ali Sina University, Hamadan, Iran.

²Department of Water Engineering, Faculty of Agriculture, Kermanshah Branch, Islamic Azad University, Kermanshah, Iran.

GRAPHICAL ABSTRACT



Article history:

Received 20 October 2021

Reviewed 9 January 2022

Received in revised form 19 February 2022

Accepted 23 February 2022

Available online 25 February 2022

Keywords:

FLOW-3D

Flow pattern

k- ϵ turbulence model

Numerical simulation

Rectangular side orifices

Article type: Research Article

In this paper, the flow in the vicinity of rectangular side orifices placed in main channels is estimated by means of the FLOW-3D model. To reconstruct the flow free surface, the volume of fluid (VOF) approach is utilized. In addition, the standard k- ϵ and RNG k- ϵ turbulence models are employed to predict turbulence flow. According to the results obtained from the numerical modeling, the RNG k- ϵ turbulence model has higher accuracy than the standard k- ϵ . The analysis of the numerical modeling results proved that this model forecasts the discharge coefficient of side weirs with suitable accuracy. On the other hand, the mean absolute percent error (MAPE) is calculated equal to 12.204%. Also, the maximum pressure is simulated near the main channel bed. Moreover, the minimum pressure is estimated near the flow free surface. Regarding the numerical simulations, the maximum turbulence energy state occurs near the inlet of the side orifice and by increasing the side orifice dimensions the flow field turbulence energy value increases.



© The Author (s)

Publisher: Razi University

1. Introduction

Due to the importance of side orifices, numerous investigations have been done on these hydraulic structures. For instance, Ramamurthy et al. (1986), Ramamurthy et al. (1987), Gill (1987), Oliveto et al. (1997), Hussein et al. (2010), Hussein et al. (2011), Bazanehet al. (2016), Ebrahimzadeh et al. (2018), Azimi and Shabanlou (2017, 2018), Shabanlou et al. (2019), studied the flow pattern in main flumes placed along the side orifices. In recent decades, the utilization of

numerical models for simulating the flow pattern has increased significantly. Convenient use and reducing expenses are the most important benefits of numerical models. Therefore, numerous numerical studies regarding the simulation of the flow have been done by different researchers. For instance, Qu (2005) by means of the k- ω turbulence model and the VOF method presented a numerical simulation for forecasting the 3D flow. He compared the pressure distribution of the computational field with the experimental data. Karizi and Honar (2008) simulated the flow passing over a broad-edged side

*Corresponding author Email: mheydari@basu.ac.ir

weir in 2D and 3D cases using FLUENT and also the k-ε turbulence model as well as the rigid bed approach. They compared the shear stress resulted by the numerical simulation with their own experimental studies. In addition to confirming the numerical model capability in simulating the flow pattern, they asserted that round-edged inputs significantly decrease shear stress induced to outer and inner walls. Furthermore, Tadayon (2009) presented a model using different turbulence models and the VOF method. He simulated the flow field across the side orifice and the flow properties. Aydin (2012) modeled the flow field upon a rectangular flume with labyrinth triangular side weir using FLUENT. He simulated the flow field surface across the side weir using different turbulence models. In addition, Aydin and Emiroglu (2013) by means of different turbulence models and the VOF scheme estimated the discharge coefficient of labyrinth side weirs. In their study, the discharge coefficient of side weirs was predicted by the numerical model and compared with experimental measurements. Azimi et al. (2014) estimated velocity and free surface in a circular canal equipped by a side weir. They showed that flow surface enhanced along the side weir. Moreover, Azimi et al. (2015) modeled the discharge coefficient of side weirs within circular flumes using an analytical approach and a numerical model. Azimi and Shabanlou (2015) predicted the water in triangular channels with side weirs. They investigated the effects of the Froude number on flow characteristics. Additionally, Azimi et al. (2016) simulated the water behavior in circular channels along a side weir by using a numerical model. They provided some linear regression models to calculate the discharge coefficient. In addition, Azimi et al. (2017) simulated the discharge coefficient of the rectangular side orifices by using a computational fluid dynamics model and a hybrid artificial intelligence approach. Akbari et al. (2017) predicted the discharge coefficient of labyrinth weirs by means of two artificial intelligence methods including M5' and the neural network. The authors showed that the M5' model had better performance.

Side orifices are utilized to divert and conduct the flow in main channels. These structures are widely used in drainage-irrigation networks, sewage disposal systems and other hydraulic projects. In contrast, thanks to the saving time and laboratory costs, the application of numerical models is increasing. Furthermore, the FLOW-3D software is one of the most powerful applicable tools in simulating the flow field within hydraulic structures. In this study, the computational field near rectangular side orifices is modeled. After that, the influence of the dimensions of this type of side orifices on the flow pattern in the main channel is evaluated. To this end, turbulence of the computational field is modeled by the existing models and the changes of the flow free surface are reconstructed by the VOF method.

2. Materials and methods

2.1. Experimental Model

To verify the results from the numerical simulation, the experimental measurements reported by Hussein et al. (2011) are employed. Hussein et al. (2011)'s experimental model is consisted of a rectangular flume with the length, width and height of 9.15m, 0.5m and 0.6m, respectively. To adjust the flow inside the channel, a gate was installed at the end of the main channel. The range of the measurements is given in Table1. In Table1, Q_m represents the discharge within the main flume, Q is the side orifice discharge, L is the width of side orifice, Y_m is the flow depth inside the main flume, V_i is velocity inside the main flume, W is the bottom height of the side orifice from the flume bed and the Fris the flow Froude number.

Table 1. Range of Hussein et al. (2011) experimental measurements.

Parameter	Range
$F_r(-)$	0.05-0.48
$W(m)$	0.05-0.2
$V_i(m/s)$	0.12-0.79
$Y_m(m)$	0.154-0.590
$L(m)$	0.044-0.133
$Q(m^3/s)$	0.0009-0.0288
$Q_m(m^3/s)$	0.1467-0.281

2.2. Governing Equations

To model the computational field the continuity and averaged Navier-Stocks equations are used (Azimi et al. 2017).

$$V_F \frac{\partial \rho}{\partial t} = \frac{\partial(\rho u A_x)}{\partial x} + \frac{\partial(\rho v A_y)}{\partial y} + \frac{\partial(\rho w A_z)}{\partial z} = R_{SOR} \tag{1}$$

$$\frac{\partial u}{\partial t} + \frac{1}{V_F} \left[u A_x \frac{\partial u}{\partial x} + v A_y \frac{\partial u}{\partial y} + w A_z \frac{\partial u}{\partial z} \right] = -\frac{1}{\rho} \frac{\partial P}{\partial x} + G_x + f_x \tag{2}$$

$$\frac{\partial v}{\partial t} + \frac{1}{V_F} \left[u A_x \frac{\partial v}{\partial x} + v A_y \frac{\partial v}{\partial y} + w A_z \frac{\partial v}{\partial z} \right] = -\frac{1}{\rho} \frac{\partial P}{\partial y} + G_y + f_y \tag{3}$$

$$\frac{\partial w}{\partial t} + \frac{1}{V_F} \left[u A_x \frac{\partial w}{\partial x} + v A_y \frac{\partial w}{\partial y} + w A_z \frac{\partial w}{\partial z} \right] = -\frac{1}{\rho} \frac{\partial P}{\partial z} + G_z + f_z \tag{4}$$

Here, (u, v, w) , (G_x, G_y, G_z) and (f_x, f_y, f_z) are velocity components, fractional area to the flow, gravitational forces and gravitational accelerations resulted from viscosity in the (x,y,z) directions, respectively. In addition, t, ρ, R_{SOR}, P and V_F are time, fluid density, source term, pressure and a fraction of volume associated with the flow, respectively. To simulate changes of the free surface, the VOF method is employed. In this method, to compute the volumetric component of the fluid, the following transmission equation is solved (Azimi et al. 2017).

$$\frac{\partial F}{\partial t} + \frac{1}{V_F} \left[\frac{\partial}{\partial x}(F u A_x) + \frac{\partial}{\partial y}(F v A_y) + \frac{\partial}{\partial z}(F w A_z) \right] = 0 \tag{5}$$

In this relationship, F denotes the volumetric component of the fluid in a computational cell. If the specified cell is filled by water, so $F=1$, if $F=0$ the cell is empty and if $0 < F < 1$ it means that the cell contains both the phases of water and air.

2.3. Boundary conditions

The boundary conditions applied for the model must be matched with the experimental model. Furthermore, based on the numerical model results, the most optimize boundary conditions are selected for the model. Thus, for the numerical model input, the certain velocity boundary conditions are taken into account. For the output of the mentioned model, the output boundary conditions are applied. The bed and sidewalls of the numerical model are also introduced as the wall boundary conditions. In addition, the top boundary of the numerical model is equivalent to the symmetry boundary conditions.

2.4. Meshing computational domain

Given that changes of the flow free surface are simulated by the VOF method, the channel height should be specified so that the considered boundary conditions for the air phase have no effect on the results. According to the study conducted by Tarek et al. (2004) in modeling changes the free surface by means of the VOF method, the initial height of the air layer can be greater than one-third of the height input flow. Thus, in the mentioned model, the initial height of the air layer is considered higher than one-third of the total height of the flow at the beginning section. This height is taken into account equal to the water height plus the air layer height. In modeling the flow field, the whole computational field is meshed by means of a non-uniform mesh block composed of rectangular cells. The sensitivity of the numerical model to the gridding procedure has always been one of the most significant problems in numerical simulations. In Figure1, the characteristics of the gridding used in the mentioned numerical model are shown. For example, the difference between gridding 3 and gridding 4 and 5 is insignificant. Thus, #3 mesh is considered for gridding the computational field. As shown, by increasing the number of the cells the mean absolute percent error of the values simulated by the numerical model is reduced dramatically. To estimate the precision of the model in predicting different parameters of the flow, the mean absolute percent error (MAPE) is obtained from Equation 6. In the equation, $(R)_{(Observed)i}$ an $(R)_{(Predicted)i}$ and n are experimental measurements, simulated values and experimental measurements, respectively:

$$MAPE = \frac{1}{n} \sum_{i=1}^n \left[\frac{|(R)_{(Predicted)i} - (R)_{(Observed)i}|}{(R)_{(Observed)i}} \right] \times 100 \tag{6}$$

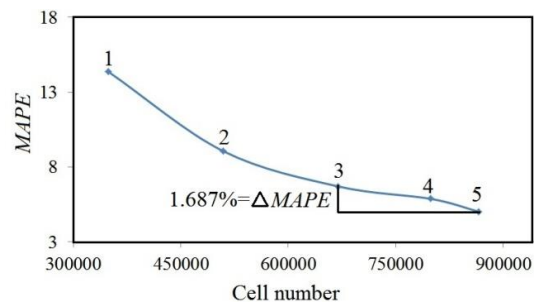


Fig. 1. Results of mesh independency.

2.5. Effects of turbulence models

One of the most important parts of numerical studies is the determination of the optimized turbulence model to simulate turbulence of the flow. The FLOW-3D comprises five different turbulence models. Two of these turbulence models include single-equation turbulence models which are of little use in practice because they do not have acceptable accuracy in flow field turbulence modeling. The LES turbulence model is also applicable by computing systems with powerful processors. Thus, only the standard k-ε (two-equation k-ε) and RNG k-ε turbulence models are classified as applicable turbulence models. FLOW-3D includes the standard k-ε (two-equation k-ε) and RNG k-ε turbulence models which in the former two kinetic energy differential equations and kinetic energy dissipation rate equations are used, while in the latter some equations similar to two-equation turbulence models equations like the k-ε model are employed. These turbulence models (RNG k-ε) are on the basis of the Reynolds normalized groups including a statistical perspective to derive an average equation for turbulence quantities. Models based on stress parameters less rely on empirical parameters. The RNG k-ε turbulence model is a sample of the turbulence models with the Reynolds normalized stress equation. In the RNG k-ε turbulence model, equations similar to the equations of the k-ε model are employed, but constant values of the RNG k-ε model are computed explicitly. Constants of the k-ε turbulence model are computed empirically. In this paper, the influence of the standard k-ε and RNG k-ε turbulence models on the numerical simulation outcomes is examined. In Table2, the MAPE values of the predicted discharge coefficient results for the standard k-ε and RNG k-ε turbulence models are listed. Based on the modeling outcomes, the results of the RNG k-ε turbulence model are close to the experimental data. Thus, the RNG k-ε turbulence model is applied in the following for modeling the computational field turbulence.

Table 2. Turbulence models sensitivity.

Turbulence Model	MAPE
Standard k-ε	9.34
RNGk-ε	6.71

2.6. Validation of numerical model results

In the following, the numerical model results in simulating the discharge coefficient of side orifices are compared with the experimental measurements reported by Hussein et al. (2011). According to the numerical simulations, the average value of MAPE for the numerical models is obtained to be 12.204%. Then, the side orifice discharge coefficient predicted by the numerical model is compared with various experimental values and the results are given in Table 3. Based on the computed criteria, the numerical model simulates the discharge of side weir with reasonable precision.

2.7. Flow pattern

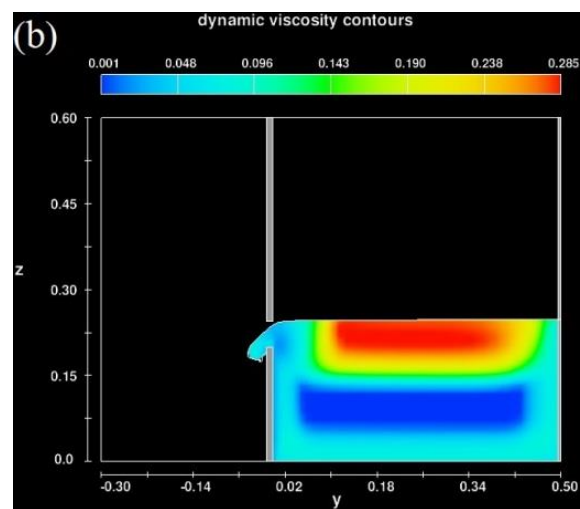
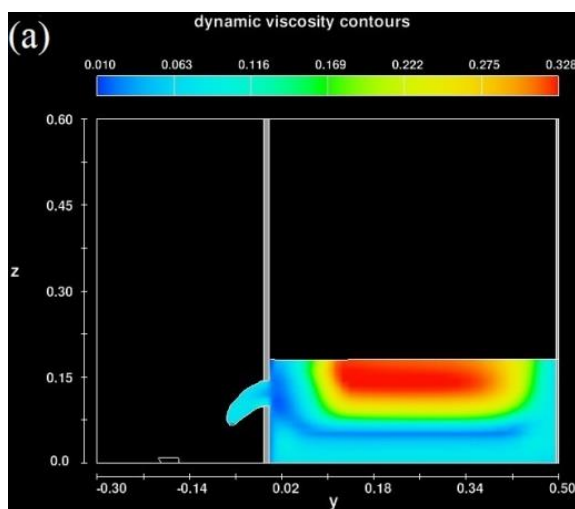
In the following, the effects of the side orifice dimensions (L) and the bottom height of the side orifice from the flume bottom (W) on the

turbulent flow properties are studied. First, the effects of the mentioned parameters on the dynamic viscosity are evaluated. In Fig. 2, the changes of the flow field dynamic viscosity in the vicinity of the orifice for the models L=0.044 m, W= 0.1 m; L=0.044 m, W= 0.2 m; L=0.089 m, W= 0.1 m and L=0.089 m, W= 0.05 m are extracted. As can be seen, the maximum value of the dynamic viscosity is predicted near the free surface on the central axis in the main channel. In all models, the minimum value of the mentioned hydrodynamic parameter occurs near the rectangular side weir inlet.

Table 4. Comparison of modeled discharge of rectangular side weir with experimental values.

Q _(exp)	Q _(num)	MAPE, %
0.00213	0.0028	31.4554
0.00369	0.0046	24.66125
0.00131	0.0016	22.1374
0.00202	0.0023	13.86139
0.00206	0.00173	16.01942
0.00149	0.00163	9.395973
0.00099	0.0009	9.090909
0.01381	0.0159	15.13396
0.01189	0.0142	19.42809
0.00865	0.0087	0.578035
0.00917	0.01	9.051254
0.01028	0.0106	3.11284
0.01334	0.0121	9.295352
0.00915	0.0107	16.93989
0.01194	0.0124	3.852596
0.00991	0.0087	12.20989
0.01196	0.0127	6.187291
0.00631	0.007	10.93502
0.00921	0.0098	6.40608
0.01246	0.013	4.333868

In the following, the influences of changes of geometric properties, side orifice length and its crest height on the changes of the volumetric component of the fluid are investigated. As discussed above, the VOF scheme is used for simulating flow free surface variations. In this study, two fluids (air and water) are considered for simulating the flow pattern inside rectangular channels with side orifice. In the continuity equation related to the VOF scheme, the value of F varies from zero to one. In other words, by solving the flow field, the computational cells with F=0 are filled with air, while if F is predicted equal to one, the interested cell is filled with water. It is worth noting that in this study, the value of F at the interaction point of the air and water layers is assumed to be 0.5. In Fig. 3, the reconstruction trend of the layer in common of the fluids for the numerical models L=0.044 m, W= 0.1 m; L=0.044 m, W= 0.2 m; L=0.089 m, W= 0.1 m and L=0.089 m, W= 0.05 m is illustrated. As shown, the value of F inside the main channel is predicted equal to one, while this value in the top layers of the water within the main flume is predicted to be zero. In all numerical models, the value of the mentioned factor is predicted to be about 0.5.



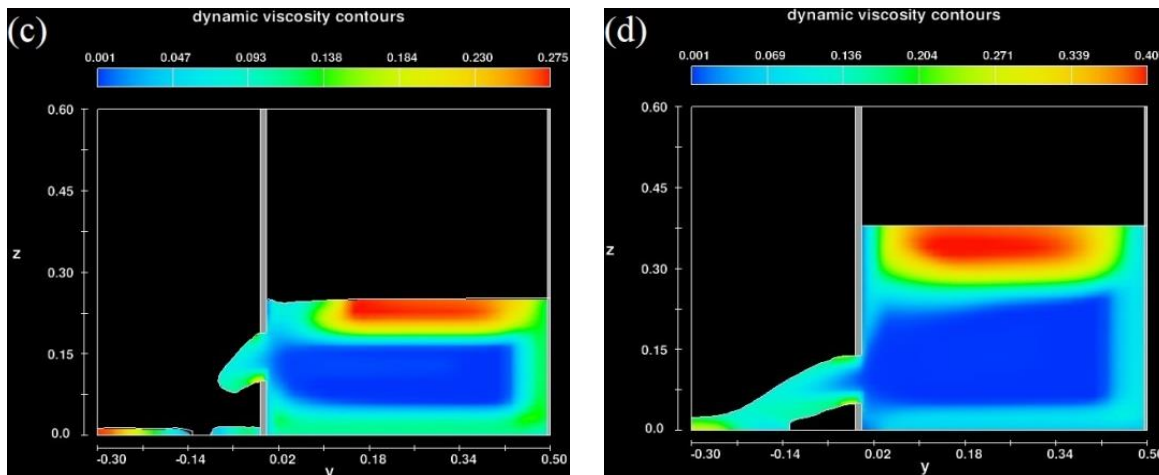


Fig. 2. Variations of flow field dynamic viscosity pattern in the vicinity of side orifice (a) $L=0.044$ m, $W=0.1$ m; (b) $L=0.044$ m, $W=0.2$ m; (c) $L=0.089$ m, $W=0.1$ m; (d) $L=0.089$ m, $W=0.05$ m.

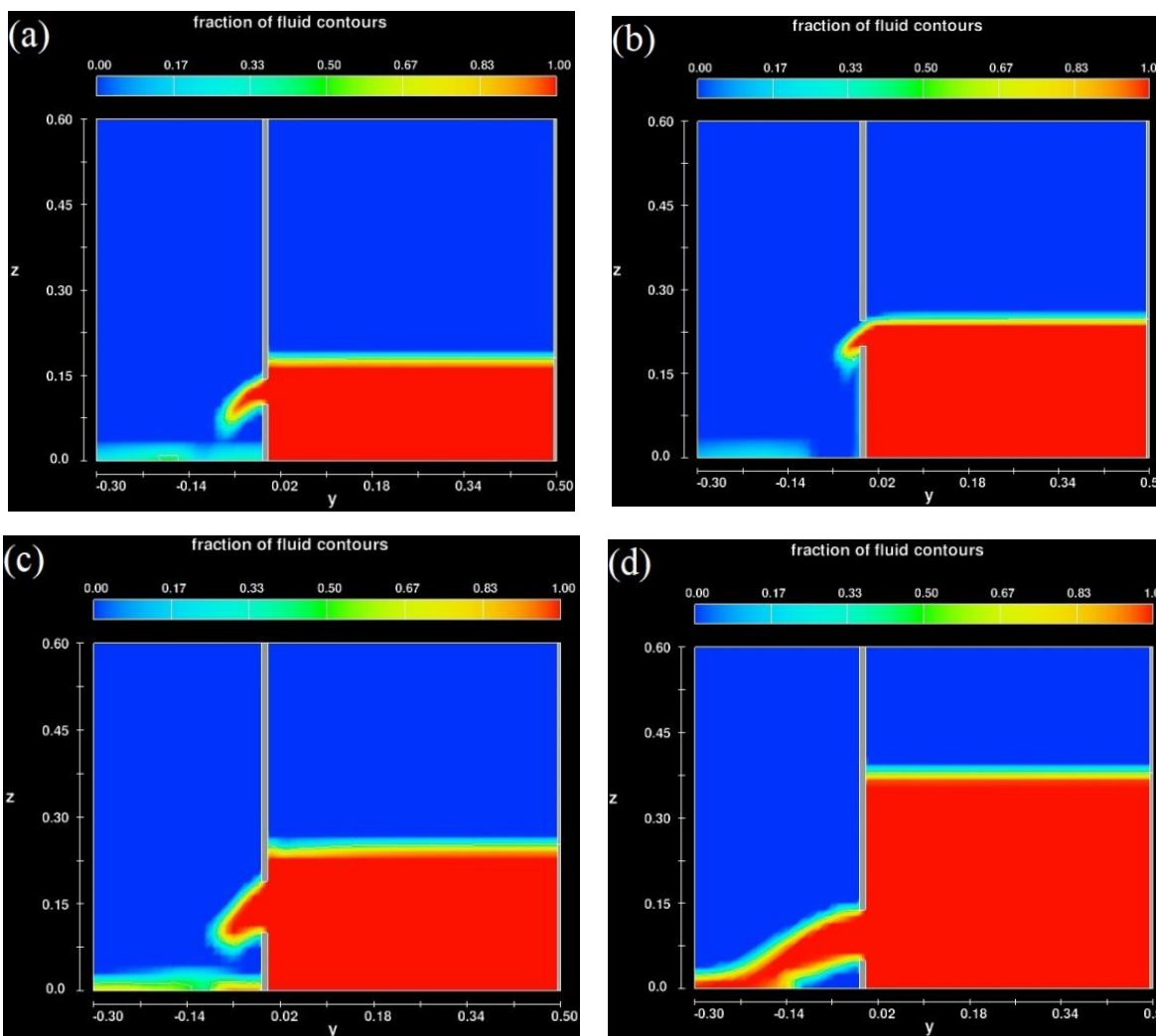


Fig. 3. Changes of volumetric component of air and water of the flow near side orifice (a) $L=0.044$ m, $W=0.1$ m; (b) $L=0.044$ m, $W=0.2$ m; (c) $L=0.089$ m, $W=0.1$ m; (d) $L=0.089$ m, $W=0.05$ m.

The influences of the side orifice length and its crest height on the pressure of the computational field are also evaluated. In Fig. 4, the effects of the parameters W and L on the changes of the flow field are illustrated. As shown, the maximum values of the flow field pressure inside the main channel are simulated near the rectangular flume bottom, while the minimum values of the flow field pressure in the main

flume are estimated near the free surface. It should be noted that the flow pressure value at the inlet of the side orifice is predicted as negative. The reason of the existence of such negative values in the mentioned regions is the presence of the negative velocity gradient. Thus, the hydrodynamic pressure in the vicinity of the side orifice is subsequently modeled negatively.

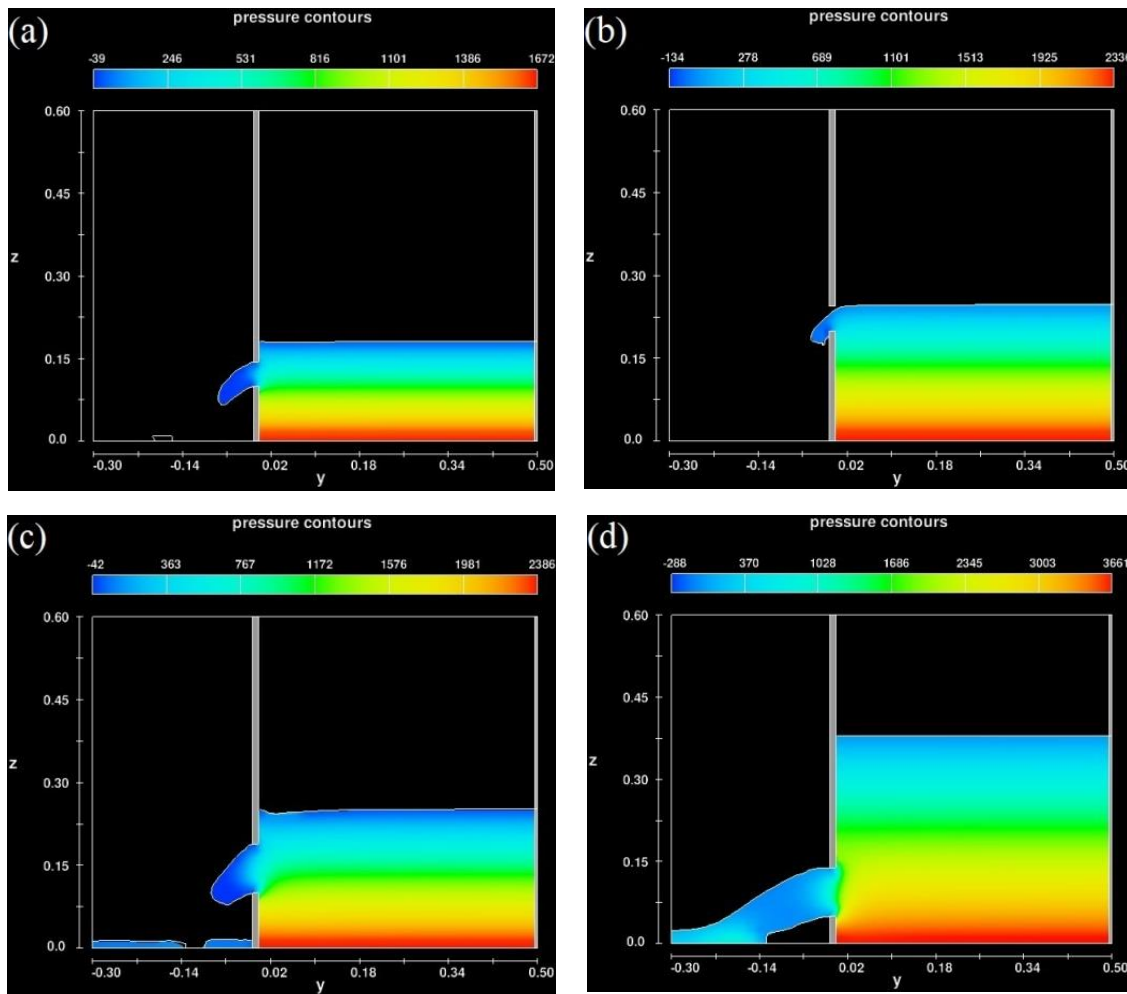
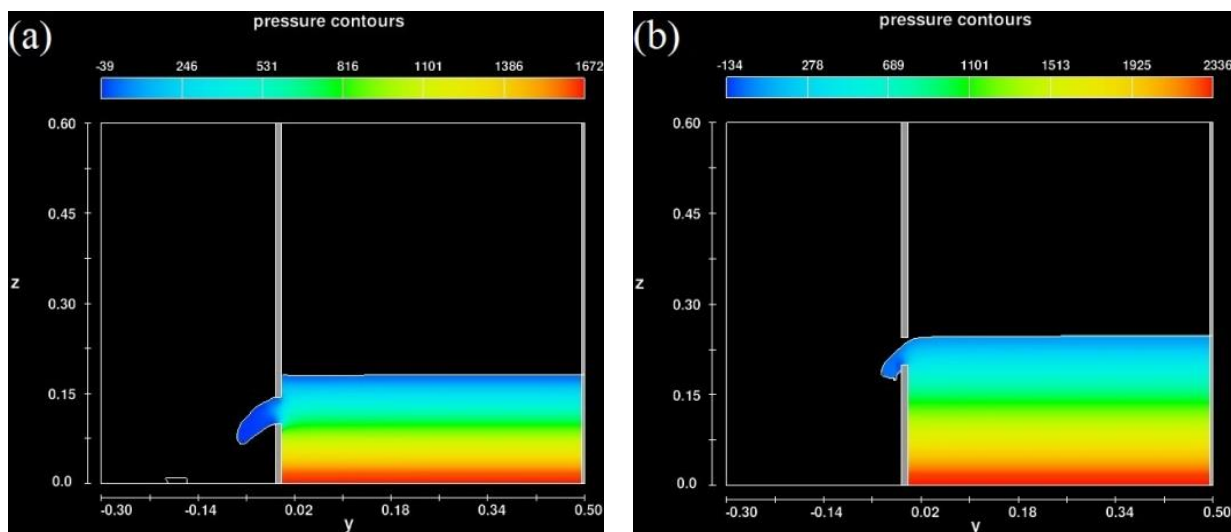


Fig. 4. Changes of flow field pressure near side orifice (a) $L=0.044$ m, $W= 0.1$ m; (b) $L=0.044$ m, $W= 0.2$ m; (c) $L=0.089$ m, $W= 0.1$ m; (d) $L=0.089$ m, $W= 0.05$ m.

In the following, the changes of the shear stress of the computational field near the inlet of the rectangular side orifice for the numerical models $L=0.044$ m, $W= 0.1$ m; $L=0.044$ m, $W= 0.2$ m; $L=0.089$ m, $W= 0.1$ m and $L= 0.089$ m, $W= 0.05$ m are studied. Fig. 5 displays the changes of shear stress for the mentioned numerical model. Based on the modeling results, the maximum of the shear stress

is forecasted near the edges of the orifice. For example, the value of the variable for the model $L=0.044$ m, $W= 0.1$ m is calculated equal to 4.07 Pa, while this value for the model $L=0.089$ m, $W= 0.1$ m is approximated to be 6.14 Pa. Thus, shear stress increases by increasing the dimensions of the rectangular side orifice.



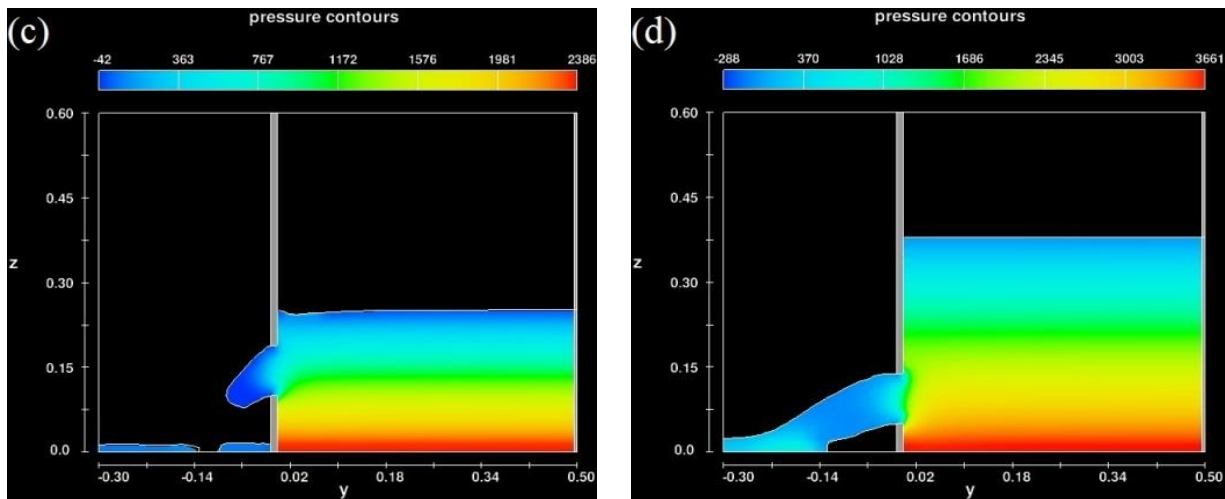


Fig. 5. Changes of shear stress pattern near side orifice crest (a) $L=0.044$ m, $W= 0.1$ m; (b) $L=0.044$ m, $W= 0.2$ m; (c) $L=0.089$ m, $W= 0.1$ m; (d) $L=0.089$ m, $W= 0.05$ m.

In addition, the influences of the W and L values on the changing pattern of turbulence drop of the flow field at the inlet of the side orifice are evaluated. The changing pattern of turbulence drop of the water near the orifice for different introduced models in the previous sections is shown in Figure 6. Based on the numerical simulation outputs, the maximum of the mentioned parameter occurs near the side orifice. For example, for the model with $L=0.044$ m, $W= 0.1$ m, the maximum value of flow field turbulence drop is computed to be $0.095 \text{ m}^2/\text{s}^3$, while for the model with $L=0.089$ m, $W= 0.1$ m, the maximum value of this parameter is obtained equal to $0.154 \text{ m}^2/\text{s}^3$. Therefore, by increasing the side

orifice dimensions, the maximum turbulence drop value increases. In this section, the changes of turbulence energy of the computational field at the inlet of the side orifice for the models $L=0.044$ m, $W= 0.1$ m; $L=0.044$ m, $W= 0.2$ m; $L=0.089$ m, $W= 0.1$ m and $L=0.089$ m, $W= 0.05$ m are shown in Fig. 7. Similar to the changing pattern of flow turbulence drop, the maximum turbulence energy occurs near the inlet of the rectangular side orifice. Also, according to the mentioned figure, by increasing the side orifice dimensions, the flow field turbulence energy value increases.

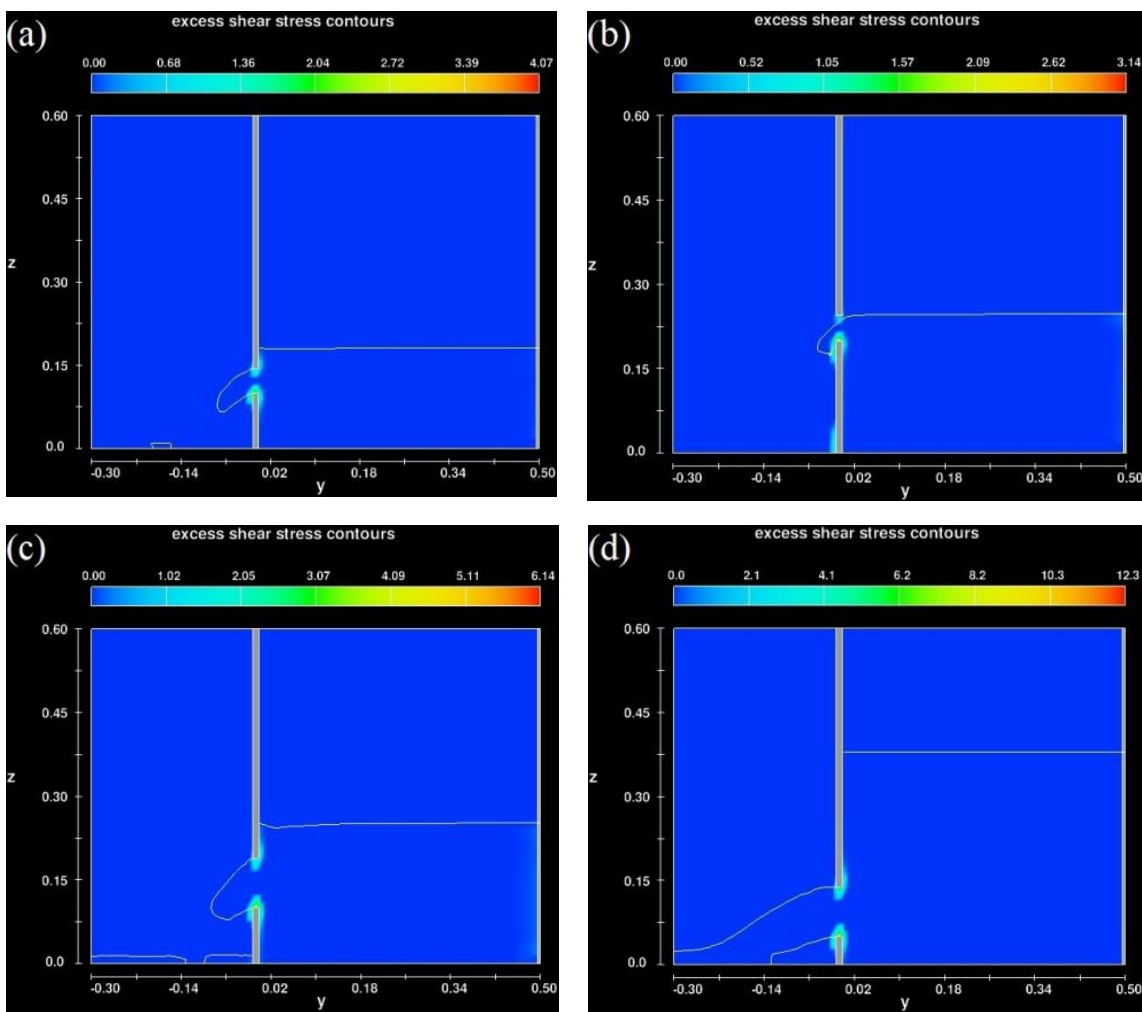


Fig. 6. Changing pattern of turbulence drop of flow field in the vicinity of side orifice (a) $L=0.044$ m, $W= 0.1$ m; (b) $L= 0.044$ m, $W= 0.2$ m; (c) $L=0.089$ m, $W= 0.1$ m; (d) $L= 0.089$ m, $W= 0.05$ m.

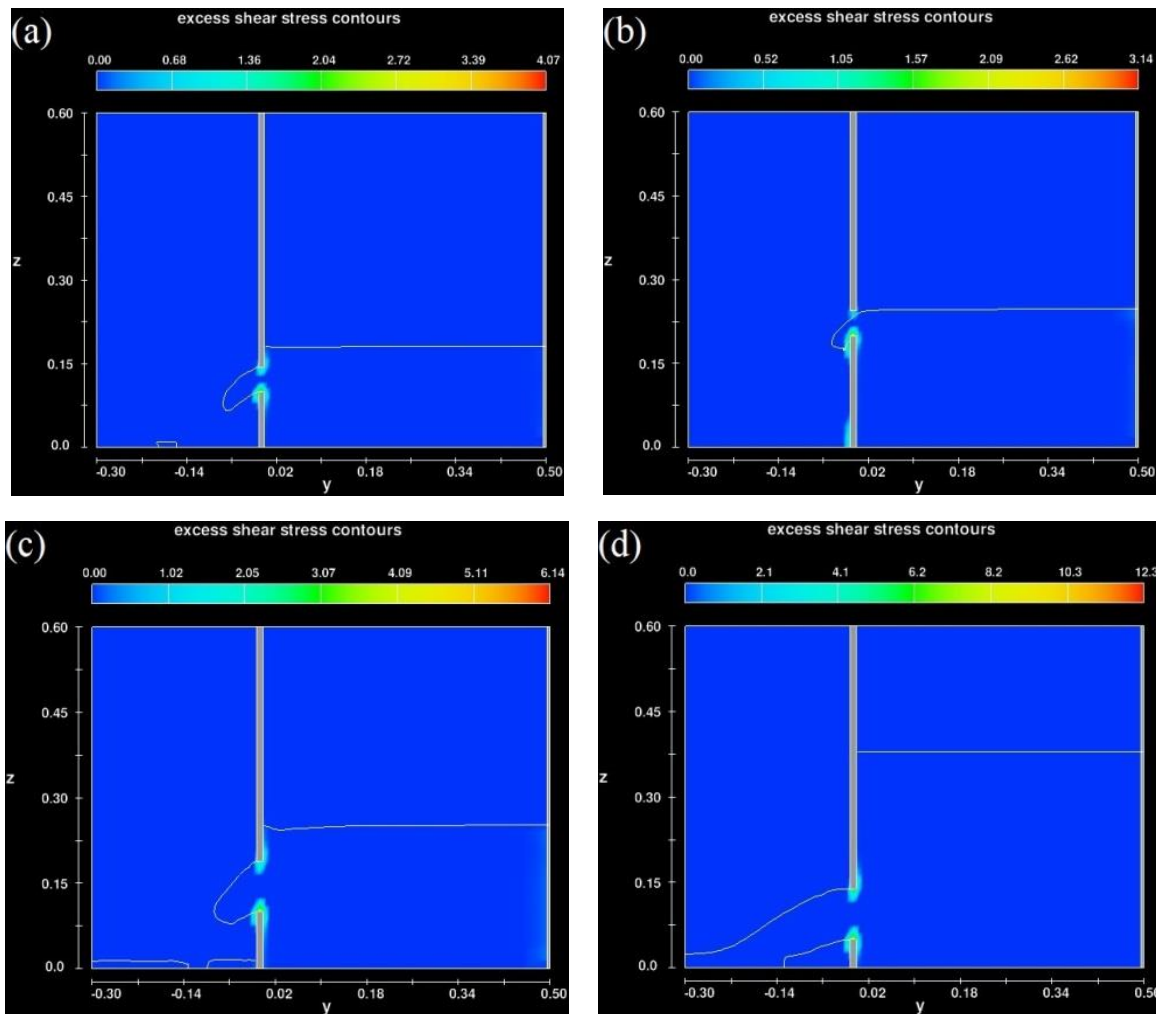


Fig. 7. Changing pattern of flow field turbulence energy in the vicinity of side orifice (a) $L=0.044$ m, $W=0.1$ m; (b) $L=0.044$ m, $W=0.2$ m; (c) $L=0.089$ m, $W=0.1$ m; (d) $L=0.089$ m, $W=0.05$ m.

4. Conclusions

In this paper, the results of the RNG $k-\epsilon$ turbulence model were close to the experimental measurements. Thus, the RNG $k-\epsilon$ turbulence model was chosen for modeling the turbulence of the flow in the rectangular channels along the side orifices. Based on the numerical model results, the average value of MAPE for the numerical models was computed to be 12.204%. Based on the calculated statistical indices, the numerical model predicted the discharge values of the orifice with reasonable precision. The effects of the side orifice length and its crest height on the computational field pressure were also evaluated and the values of the maximum flow field pressure value was simulated inside the main channel near the rectangular flume bottom, while the minimum flow pressure value was estimated in the main flume near the free surface. Based on the modeling results, the maximum shear stress value was forecasted near the edges of the orifice. For example, the value of the mentioned variable for the model with $L=0.044$ m, $W=0.1$ m was computed 4.07 Pa. The maximum value of the flow field turbulence energy occurred near the inlet of the rectangular side orifice. Furthermore, it should be noted that by increasing the side orifice dimensions, the flow field turbulence energy increases. In the current study, the flow pattern around the rectangular side orifices has evaluated so it is suggested that more experimental and numerical studies on the hydraulics of side orifices with different shapes should be done.

Acknowledgments

This research and the paper have been carried out with the help of the research assistant of the Faculty of Agriculture of Bu Ali Sina University, and we hereby appreciate them.

References

Akhbari A., Zaji A.H., Azimi H., Vafaeifard M., Predicting the discharge coefficient of triangular plan form weirs using radian basis function and M5 methods, *Journal of Applied Research in Water and Wastewater* 4 (2017) 281-289.

Aydin M.C., CFD simulation of free-surface flow over triangular labyrinth side weir, *Advances in Engineering Software* 45 (2012) 159-166.

Aydin M.C., and Emiroglu M.E., Determination of capacity of labyrinth side weir by CFD, *Flow Measurement and Instrumentation* 29 (2013) 1-8.

Azimi H., and Shabanlou S., Numerical study of the effect of the bed slope change of circular channel on supercritical flow along the side weir, *Water and Soil Science* 27 (2017) 53-64.

Azimi H., and Shabanlou S., 3D Simulation of Supercritical Flow Characteristics in Circular Channels with Side Weirs, *Water and Soil Science* 28 (2018) 119-130.

Azimi H., Shabanlou S., Salimi M.S., Free surface and velocity field in a circular channel along the side weir in supercritical flow conditions, *Flow Measurement and Instrumentation* 38 (2014) 108-115.

Azimi H., Hadad H., Shokati Z., Salimi M.S., Discharge and flow field of the circular channel along the side weir, *Canadian Journal of Civil Engineering* 42 (2015) 273-280.

Azimi H., and Shabanlou S., The flow pattern in triangular channels along the side weir for subcritical flow regime, *Flow Measurement and Instrumentation* 46 (2015) 170-178.

Azimi H., Shabanlou S., Ebtehaj I., Bonakdari, H., Discharge coefficient of rectangular side weirs on circular channels, *International Journal of Nonlinear Sciences and Numerical Simulation* 17 (2016) 391-399.

Azimi H., Shabanlou S., Ebtehaj I., Bonakdari H., Kardar S., Combination of computational fluid dynamics, adaptive neuro-fuzzy inference system, and genetic algorithm for predicting discharge

- coefficient of rectangular side orifices, *Journal of Irrigation and Drainage Engineering* 143 (2017) 04017015.
- Bazaneh M., Khorsand A., Zeinalzadeh K., Besharat S., Evaluation of HYDRUS 2D software to estimate stored water and wetting pattern of surface drip irrigation, *Water and Soil Science* 26 (2016) 287-301.
- Ebrahimzadeh A., Ziaei A., Jafarzadeh M., Beheshti A., Sheikh Rezazadeh Nikou N., Numerical modeling of one-dimensional flow in furrow irrigation by solving the full hydrodynamics equations using roe approach, *Water and Soil Science* 28 (2018) 41-51.
- Hussein A., Ahmad Z., Asawa G.L., Discharge characteristics of sharp-crested circular side orifices in open channels, *Flow Measurement and Instrumentation* 21 (2010) 418-424.
- Hussein A., Ahmad Z., Asawa G.L., Flow through sharp-crested rectangular side orifices under free flow condition in open channels, *Agricultural Water Management* 98 (2011) 1536-1544.
- Karizi A., and Honar T., Study of flow pattern and shear stress of broad edge rectangular side weir, *Journal of agricultural and natural resources sciences and technology, Soil and water sciences* 14 (2008) 15-25.
- Oliveto G., Biggiero V., Hager W.H., Bottom outlet for sewers, *Journal of Irrigation and Drainage Engineering* 123 (1997) 246-252.
- Qu J., Three-dimensional turbulence modeling for free surface flows. PhD thesis, Concordia University, Montreal, Quebec, Canada (2005).
- Ramamurthy A.S., Udoyara S.T., Serraf S., Rectangular lateral orifices in open channel, *Journal of Environmental Engineering* 135 (1986) 292-298.
- Ramamurthy A.S., Udoyara S.T., Rao M.V.J., Weir orifice units for uniform flow distribution, *Journal of Environmental Engineering* 113 (1987) 155-166.
- Shabanlou S., Yosefvand F., Azimi H., Ebtehaj I., Modeling discharge coefficient of rectangular side orifices, *Water and Soil Science*, 29 (2019) 83-96.
- Tadayon R., Modeling Curvilinear Flows in Hydraulic Structures. PhD thesis, Concordia University, Montreal, Quebec, Canada (2009).
- Tarek M., Imran J., Chaudhry H., Numerical modeling of three-dimensional flow field around circular piers, *Journal of Hydraulic Engineering* 130 (2004) 91-100.